

# $\pi$ - $\pi$ interactions between benzene and graphene by means of large-scale DFT-D4 calculations

Amir Karton

School of Molecular Sciences, The University of Western Australia, Perth, WA 6009, Australia

## ARTICLE INFO

### Keywords:

Density functional theory  
Dispersion  
Graphene  
 $\pi$ - $\pi$  interactions

## ABSTRACT

The adsorption of aromatic molecules on graphene is essential for many applications. This study addresses the issues associated with predicting accurate binding energies between graphene and benzene using a series of increasingly larger nanographene ( $C_{24}H_{12}$ ,  $C_{54}H_{18}$ ,  $C_{96}H_{24}$ ,  $C_{150}H_{30}$ , and  $C_{216}H_{36}$ ). For this purpose, we consider several DFT methods developed for accurately predicting noncovalent interactions, namely, PBE0-D4,  $\omega$ B97X-D4, PW6B95-D4, and MN15. The  $C_{150}H_{30}$  and  $C_{216}H_{36}$  nanographene predict binding energies converged to sub-kJ mol<sup>-1</sup> with respect to the size of the nanographene. For the largest  $C_{216}H_{36}$  nanographene, we obtain binding energies of -37.9 (MN15), -39.7 ( $\omega$ B97X-D4), -40.7 (PW6B95-D4), and -49.1 (PBE0-D4) kJ mol<sup>-1</sup>. Averaging these values, we obtain  $\Delta E_{e,bind} = -41.8 \pm 8.6$  kJ mol<sup>-1</sup>, which translates to  $\Delta H_{0,bind} = -41.0 \pm 8.6$  kJ mol<sup>-1</sup>. This theoretical binding energy agrees with the experimental value of  $-48.2 \pm 7.7$  kJ/mol within overlapping uncertainties.

## 1. Introduction

The adsorption of aromatic molecules on single-layer graphene via  $\pi$ - $\pi$  interactions has attracted significant attention in recent years. Such adsorption processes are essential for a wide range of potential applications of graphene in nanobiomedicine, lubrication, molecular sensing, and molecular separation [1,2,3,4,5,6,7,8]. A fundamental quantity of importance to all these processes is the interaction energy between graphene and aromatic molecules [9,10]. Over the past two decades, significant effort has been dedicated to calculating the  $\pi$ - $\pi$  interaction energy between graphene and the archetypal aromatic hydrocarbon benzene [11,12,13,14,15,16,17,18,19,20,21,22]. Chakarova-Käck et al. used the vdW-DF [23] dispersion corrected density functional theory (DFT) method and obtained binding energy of -47.8 kJ mol<sup>-1</sup> between benzene and graphene [11]. Björk et al. calculated the binding energies between graphene and a wide range of aromatic and antiaromatic molecules. [12] For benzene, they obtained binding energies of -46.8 and -55.5 kJ mol<sup>-1</sup> using the vdW-DF and Tkatchenko-Scheffler [24] dispersion corrected DFT methods. Ershova et al. obtained binding energy of -45.3 kJ mol<sup>-1</sup> at the  $\omega$ B97X-D/6-31G\* level of theory, where graphene was modeled using a large hydrogen capped nanographene consisting of 116 carbon atoms. [13] Wangmo et al. calculated lower binding energy of -42.7 kJ mol<sup>-1</sup> using density-functional tight-binding (DFTB) [14]. However, Kozlov et al. reported a substantially higher

binding energy of 78.7 kJ mol<sup>-1</sup> at the PBE-D level of theory [15]. Berland and Hyldgaard used several dispersion corrected DFT approaches and obtained binding energies ranging between -32.8 and -63.7 kJ mol<sup>-1</sup> [16]. Lechner and Sax used a nanographene consisting of 90 carbon atoms to estimate the benzene-graphene binding energy to be -44.0 kJ mol<sup>-1</sup> at the B3LYP-D2/Def2-SVP level of theory [17]. The same authors also reported a slightly lower binding energy of -42.0 kJ mol<sup>-1</sup> obtained from dispersion-corrected DFTB calculations [18].

Recently, Zhang et al. used atomic force microscope measurements to elucidate the mechanism by which a single phenyl ring is desorbed from graphene [19,20]. They found that the desorption process comprises of two steps (i) the phenyl ring rotates from a parallel to a vertical orientation relative to the graphene plane, and (ii) the phenyl ring moves upwards in a perpendicular orientation until it dissociates. An experimental binding energy between benzene and graphene can be estimated from thermal desorption spectroscopy of benzene from the basal plane of highly oriented pyrolytic graphite (HOPG) at ultra-high vacuum [21]. These experiments result in a binding energy of  $-48.2 \pm 7.7$  kJ mol<sup>-1</sup> for benzene on graphite and give a point of reference for the benzene-graphene system. We note that a similar binding energy of -46.4 kJ mol<sup>-1</sup> was obtained in an earlier experimental study for the benzene/graphite system [22]. Three issues that complicate a comparison between the experimental and theoretical binding energies are (i) the use of HOPG rather than single-layer graphene in the experiments,

E-mail address: [amir.karton@uwa.edu.au](mailto:amir.karton@uwa.edu.au).

<https://doi.org/10.1016/j.chemphys.2022.111606>

Received 19 February 2022; Received in revised form 27 April 2022; Accepted 4 June 2022

Available online 9 June 2022

0301-0104/© 2022 Elsevier B.V. All rights reserved.

(ii) the potential presence of defects in HOPG which may affect the binding energy with benzene, and (iii) the relatively large uncertainty of  $7.7 \text{ kJ mol}^{-1}$  associated with the more recent experimental binding energy.

The above computational predictions for the binding energy between a single benzene molecule and graphene spread over a wide range, i.e., the calculated binding energies range from about  $-30$  to  $-80 \text{ kJ mol}^{-1}$ . Thus, it is of interest to determine this binding energy using (i) the recently developed DFT-D4 dispersion model with DFT methods from the upper rungs of Jacob's Ladder, (ii) sufficiently large basis sets with basis-set superposition error corrections, and (iii) sufficiently large nanographene models. In the present work, we set out to calculate the binding energy between nanographene and a single benzene molecule adsorbed parallel to the nanographene plane. To obtain reliable binding energies, we use four different dispersion corrected DFT methods from the upper rungs of Jacob's Ladder. Namely, the global hybrid generalized gradient approximation (GGA) PBE0-D4 [25,26], range-separated hybrid  $\omega$ B97X-D4, [27] hybrid-meta GGA PW6B95-D4 [28], and hybrid-meta nonseparable gradient approximation (NGA) MN15 [29]. The PBE0,  $\omega$ B97X, and PW6B95 functionals are used in conjunction with the recently developed density and charge-dependent D4 dispersion correction [30,31]. Whereas the MN15 hybrid-meta NGA method incorporates dispersion interactions into the parametrization of the functional. The selected exchange–correlation functionals have been extensively benchmarked and found to be robust for dispersion interactions in related systems [29,30,31,32,33,34,35,36,37,38]. In particular, it is worth mentioning that PW6B95-D3 and  $\omega$ B97X-D3 were found to be the best performing functionals for the large supramolecular complexes in the S30L database, including  $\pi$ – $\pi$  stacking, CH– $\pi$ , and nonpolar dispersion interactions [39]. Another goal of this work is to assess the convergence of the binding energy between benzene and nanographene with respect to the size of the nanographene. For this purpose, we consider a systematic set of increasingly larger nanographenes:  $\text{C}_{24}\text{H}_{12}$  (coronene),  $\text{C}_{54}\text{H}_{18}$  (circumcoronene),  $\text{C}_{96}\text{H}_{24}$  (circumcircumcoronene),  $\text{C}_{150}\text{H}_{30}$ , and  $\text{C}_{216}\text{H}_{36}$ . We find that converging the interaction energy to the  $\text{kJ mol}^{-1}$  level requires a nanographene with at least 96 carbon atoms.

## 2. Computational details

The geometries of all structures were fully optimized without constraints at the PBE0-D3(BJ)/6-31G(d) level of theory, where empirical D3 dispersion corrections [40] are included using the Becke–Johnson [41] damping potential (denoted by the suffix D3(BJ)). Harmonic vibrational frequencies were obtained at the same level of theory and all the monomers and dimers were verified to be equilibrium structures (i.e., have all real harmonic frequencies).

In order to obtain accurate binding energies between nanographene and benzene, single-point energy calculations were carried out using two hybrid GGA methods PBE0-D4 and  $\omega$ B97X-D4 [25,26,27], and two hybrid-meta GGA/NGA methods PW6B95-D4 and MN15 [28,29,30]. The single-point energy calculations were carried out in conjunction with the Def2-TZVP basis set [42]. Basis set superposition error (BSSE) corrections were included using the Boys–Bernardi counterpoise method [43]. As shown in Refs. [44,45], unless basis sets that are sufficiently close to the one-particle basis set limit are used, the average of the raw and counterpoise-corrected interaction energies yield the fastest basis set convergence. The binding energies reported in the main text are calculated using this procedure in conjunction with the Def2-TZVP basis set (denoted by Def2-TZVP-half-CP). The binding energies calculated with the full BSSE correction (denoted by Def2-TZVP-full-CP) are given in Table S1 of the Supporting Information. We note that the differences between the Def2-TZVP-half-CP and Def2-TZVP-full-CP binding energies are below  $1 \text{ kJ mol}^{-1}$  for PBE0-D4,  $\omega$ B97X-D4, and PW6B95-D4 methods, and below  $2 \text{ kJ mol}^{-1}$  for MN15 (for further details see Table S2 of the Supporting Information). All geometry optimizations,

frequency, and single-point energy calculations were carried out using the Gaussian 16 program suite.[46]

## 3. Results and discussion

**Nanographene models.** Nanographenes are fragments of graphene with diameters bigger than 1 nm. Nanographenes are often used as models of graphene in quantum chemical simulations [5,13,17,38,47,48,49,50,51,52,53,54,55,56,57]. This approach allows for the use of more advanced and accurate electronic structure methods than those available (or computationally affordable) in periodic boundary conditions simulations, which are often limited to dispersion-corrected GGA methods. So far, most computational investigations that use DFT methods from the last rungs of Jacob's Ladder (e.g., hybrid GGA, hybrid-meta GGA, and double-hybrid DFT methods) [5,13,17,47,48,49,50,51,52,54] considered nanographenes with up to  $\sim 100$  carbon atoms (e.g., circumcircumcoronene  $\text{C}_{96}\text{H}_{24}$ ). Here we consider a systematic set of increasingly larger nanographenes with up to 216 carbon atoms. Fig. 1 shows the nanographene models considered in the present work. We use this systematic set to evaluate the limitations of smaller nanographene models in predicting the binding energy with benzene. The largest nanographene we consider ( $\text{C}_{216}\text{H}_{36}$ ) has a diameter of  $27.1 \text{ \AA}$ , which is about an order of magnitude larger than the diameter of benzene ( $2.78 \text{ \AA}$ ).

**DFT methods.** In the present work, we fully optimize the geometries and calculate the harmonic vibrational frequencies with a PBE0-D3(BJ) hybrid GGA method [25,26,35]. The binding energies between the nanographene and benzene are refined using two hybrid GGA (PBE0-D4 and  $\omega$ B97X-D4) and two hybrid-meta GGA/NGA (PW6B95-D4 and MN15) methods. These methods have been developed to reproduce reliable thermochemical and kinetic properties and non-covalent interactions and include varying degrees of exact Hartree–Fock exchange admixtures. In particular, 25% (PBE0-D4), 28% (PW6B95-D4), and 44% (MN15). The  $\omega$ B97X-D4 range-separated functional employs 100% exact exchange for long-range and 16% for short-range interactions. In addition, dispersion interactions are taken into account via two different approaches. MN15 incorporates dispersion interactions into the parametrization of the functional, while the DFT-D4 correction depends on dynamic polarizabilities and electronic density information obtained via atomic partial charges. Importantly, the selected exchange–correlation functionals also cover the gamut from functionals that are nonempirical (PBE0), lightly/moderately empirical (PW6B95 and  $\omega$ B97X), and heavily empirical (MN15).

**Nanographene models.** Fig. 2 depicts the optimized benzene•••nanographene complexes (nanographene =  $\text{C}_{24}\text{H}_{12}$ ,  $\text{C}_{54}\text{H}_{18}$ ,  $\text{C}_{96}\text{H}_{24}$ ,  $\text{C}_{150}\text{H}_{30}$ , and  $\text{C}_{216}\text{H}_{36}$ ). In the present work, we consider the complexes in which one of the benzene carbon atoms is situated directly above the center of the hexagonal nanographene (Fig. 2). Previous theoretical investigations found that this is the most energetically stable configuration [15,52]. Let us begin by analyzing the intermolecular distances in these parallel-displaced complexes. The intermolecular separation is defined here as the distance between the plane of the carbon skeleton of the benzene ring and the nanographene carbon atom positioned directly under the center of the benzene ring. Inspection of the intermolecular distances in Fig. 2 reveals that the intermolecular separation becomes shorter by as much as  $0.056 \text{ \AA}$  when increasing the size of the nanographene from  $\text{C}_{24}\text{H}_{12}$  to  $\text{C}_{54}\text{H}_{18}$ . However, further increase in the size of the nanographene has practically no effect on the intermolecular separation. It is also interesting to note that as we move to larger benzene•••nanographene complexes, the interaction between the benzene ring and the nanographene creates a dip in the nanographene. For example, in the  $\text{C}_6\text{H}_6$ ••• $\text{C}_{216}\text{H}_{36}$  complex, the distance between the plane defined by the rim carbons of the nanographene and the plane of the central benzene ring of the nanographene is  $0.316 \text{ \AA}$ .

Table 1 lists the PBE0-D4,  $\omega$ B97X-D4, PW6B95-D4, and MN15 binding energies for the benzene•••nanographene complexes in Fig. 2

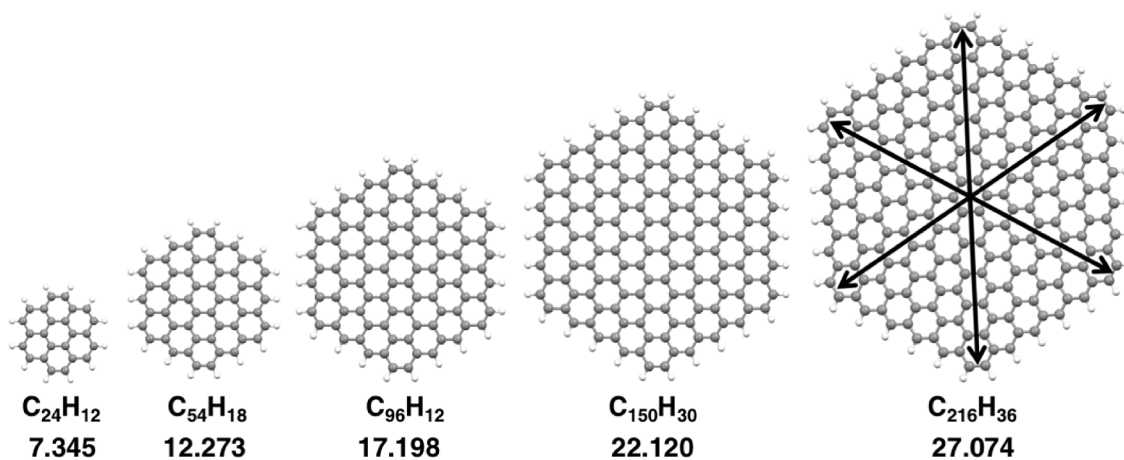


Fig. 1. Optimized structures of the nanographene models considered in this work. The diameter of the carbon skeleton is given in Å (shown for the  $C_{216}H_{36}$  structure).

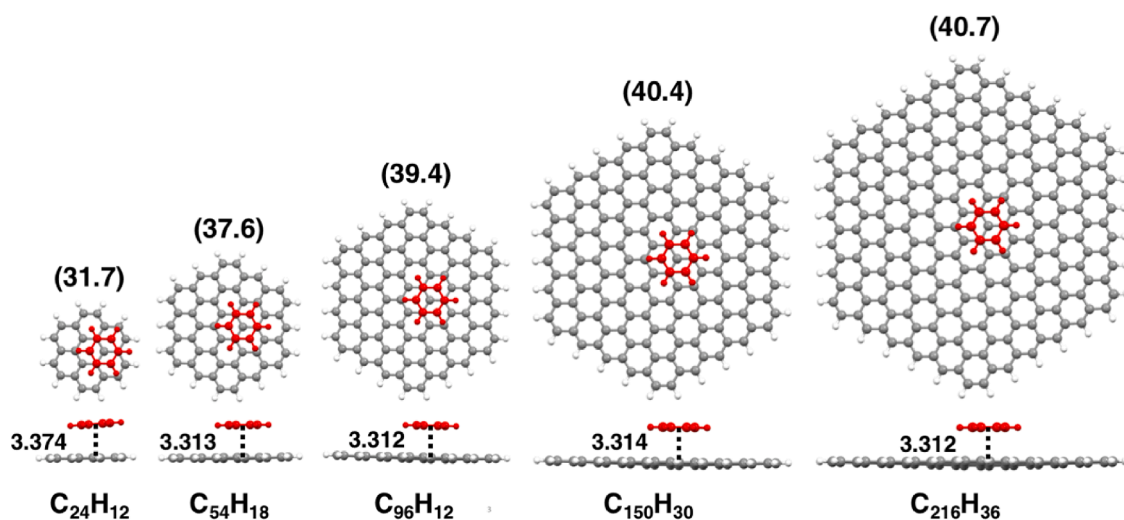


Fig. 2. Top and side views of the optimized structures of the benzene•••nanographene complexes considered in this work. The distance between the plane of the benzene ring and the nanographene is given in Å. The PW6B95-D4/Def2-TZVP-half-CP electronic binding energies are given in parentheses in  $\text{kJ mol}^{-1}$ .

Table 1

Electronic binding energies ( $\Delta E_{e,bind}$ ) for the benzene•••nanographene complexes in Fig. 2, calculated in conjunction with the Def2-TZVP basis set with a half-counterpoise BSSE correction (Def2-TZVP-half-CP, in  $\text{kJ mol}^{-1}$ ).

Nanographene	PBE0-D4	$\omega$ B97X-D4	PW6B95-D4	MN15
$C_{24}H_{12}$	-36.1	-30.8	-31.7	-34.2
$C_{54}H_{18}$	-45.4	-37.2	-37.6	-37.7
$C_{96}H_{24}$	-47.7	-39.2	-39.4	-38.0
$C_{150}H_{30}$	-48.8	-39.4	-40.4	-38.0
$C_{216}H_{36}$	-49.1	-39.7	-40.7	-37.9

(nanographene =  $C_{24}H_{12}$ ,  $C_{54}H_{18}$ ,  $C_{96}H_{24}$ ,  $C_{150}H_{30}$ , and  $C_{216}H_{36}$ ). The binding energies are also plotted in Fig. 3. It is instructive to examine the convergence of the binding energies with respect to the size of the nanographene. We begin by noting that the PW6B95-D4/Def2-TZVP-half-CP binding energy for the parallel-displaced benzene dimer ( $-11.5 \text{ kJ mol}^{-1}$ ) is in excellent agreement with the recent high-level binding energy calculated at the CCSDT(Q)/CBS level of theory of  $-10.7 \text{ kJ mol}^{-1}$  [58], CCSDT(Q)/CBS denotes coupled-cluster with singles, doubles, triples, and quasi-perturbative quadruple excitations method at the complete basis set limit [59]. The other functionals result in a larger overestimation of the CCSDT(Q)/CBS binding energy.

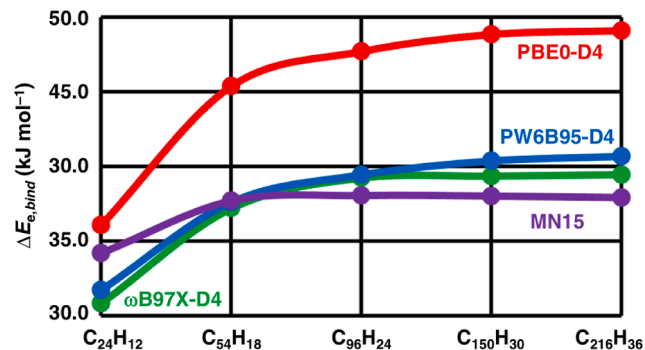


Fig. 3. Electronic binding energies ( $\Delta E_{e,bind}$ ) for the benzene•••nanographene complexes in Fig. 2 calculated in conjunction with the Def2-TZVP basis set with a half-counterpoise BSSE correction (in  $\text{kJ mol}^{-1}$ ).

Namely, we obtain binding energies of  $-12.3$  ( $\omega$ B97X-D4),  $-12.7$  (PBE0-D4), and  $-13.7$  (MN15)  $\text{kJ mol}^{-1}$ .

For the benzene••• $C_{24}H_{12}$  complex, we obtain binding energies ranging between  $-30.8$  ( $\omega$ B97X-D4) and  $-36.1$  (PBE0-D4)  $\text{kJ mol}^{-1}$ . These binding energies are nearly three times higher than that for the

benzene parallel-displaced dimer; however, they are far from being converged with respect to the size of the nanographene. In particular, for the PBE0-D4,  $\omega$ B97X-D4, and PW6B95-D4 functionals, the benzene $\bullet\bullet\bullet$ C<sub>24</sub>H<sub>12</sub> binding energies underestimate those for the benzene $\bullet\bullet\bullet$ C<sub>216</sub>H<sub>36</sub> dimer by 9–13 kJ mol<sup>-1</sup> (Table 1 and Fig. 3). Interestingly, the convergence of the binding energy with respect to the size of the nanographene is faster for the MN15 functional. The difference between the benzene $\bullet\bullet\bullet$ C<sub>24</sub>H<sub>12</sub> and benzene $\bullet\bullet\bullet$ C<sub>216</sub>H<sub>36</sub> binding energies is 3.7 kJ mol<sup>-1</sup> for the MN15 functional.

Increasing the size of the nanographene from C<sub>24</sub>H<sub>12</sub> to C<sub>54</sub>H<sub>18</sub> results in significant increases in the binding energies by 9.3 (PBE0-D4), 6.4 ( $\omega$ B97X-D4), 5.9 (PW6B95-D4), and 3.5 (MN15) kJ mol<sup>-1</sup>. These significant increases in the binding energies are not surprising given that in the benzene $\bullet\bullet\bullet$ C<sub>24</sub>H<sub>12</sub> complex, the benzene ring is not entirely surrounded by the  $\pi$ -system of the underlying nanographene as shown in the top view representation in Fig. 2. In the benzene $\bullet\bullet\bullet$ C<sub>54</sub>H<sub>18</sub> complex, on the other hand, the benzene ring is entirely surrounded by the  $\pi$ -system of the underlying nanographene (Fig. 2). Nevertheless, for the PBE0-D4,  $\omega$ B97X-D4, and PW6B95-D4 functionals, the binding energies predicted by the C<sub>54</sub>H<sub>18</sub> model system still underestimate those predicted by the most extensive C<sub>216</sub>H<sub>36</sub> model system by 2–4 kJ mol<sup>-1</sup> (Table 1 and Fig. 3). Thus, while the C<sub>54</sub>H<sub>18</sub> nanographene provides a useful estimation of the binding energy, it is deemed not sufficiently large for obtaining a reliable binding energy with benzene. As noted above, the MN15 binding energies exhibit faster convergence with respect to the size of the nanographene. As a result, the binding energies obtained for the C<sub>54</sub>H<sub>18</sub> and the larger nanographene (C<sub>96</sub>H<sub>24</sub>, C<sub>150</sub>H<sub>30</sub>, and C<sub>216</sub>H<sub>36</sub>) are practically unchanged (Table 1 and Fig. 3). This result could indicate that MN15 underestimates long-range dispersion interactions in the larger nanographene models.

The C<sub>96</sub>H<sub>24</sub> nanographene is the smallest model system that provides a chemically accurate prediction of the binding energy with benzene in the  $\sim$ 1 kJ mol<sup>-1</sup> range. In particular, the binding energy for the benzene $\bullet\bullet\bullet$ C<sub>96</sub>H<sub>24</sub> dimer underestimates that for the benzene $\bullet\bullet\bullet$ C<sub>216</sub>H<sub>36</sub> dimer by 1.4 (PBE0-D4) and 1.2 (PW6B95-D4) kJ mol<sup>-1</sup>. For the  $\omega$ B97X-D4 and MN15 functionals the binding energy for C<sub>96</sub>H<sub>24</sub> is practically converged with respect to the size of the nanographene (Table 1).

We note that the above underestimations of just over 1 kJ mol<sup>-1</sup> obtained for the PBE0-D4 and PW6B95-D4 functionals still amount to  $\sim$ 3% of the binding energy. Thus, a larger nanographene is still needed for reducing the error due to the size of the nanographene to below 1%. The binding energies obtained with the C<sub>150</sub>H<sub>30</sub> nanographene are all 0.1–0.3 kJ mol<sup>-1</sup> from those obtained with the C<sub>216</sub>H<sub>36</sub> nanographene. These deviations are smaller than 1% of the binding energy and indicate that the binding energy of the benzene $\bullet\bullet\bullet$ C<sub>216</sub>H<sub>36</sub> complex is fully converged with respect to the size of the nanographene (i.e., moving to an even larger nanographene would not result in any significant change).

The above results also show that the convergence rate with respect to the size of the nanographene differs between the selected DFT functionals, with MN15 and PBE0-D4 representing limit cases of faster and slower convergence behavior, respectively, and  $\omega$ B97X-D4 and PW6B95-D4 exhibit in-between convergence rates (Fig. 3). We expect these limit cases to be representative of a wider range of functionals since the chosen set of functionals is relatively diverse and includes range-separated hybrid, global hybrid, hybrid-meta, nonempirical, lightly empirical, and heavily empirical DFT methods.

**Best binding energies between benzene and nanographene.** For the largest nanographene (benzene $\bullet\bullet\bullet$ C<sub>216</sub>H<sub>36</sub>) we obtain electronic binding energies of  $\Delta E_{e,bind} = -37.9$  (MN15),  $-39.7$  ( $\omega$ B97X-D4),  $-40.7$  (PW6B95-D4), and  $-49.1$  (PBE0-D4) kJ mol<sup>-1</sup>. Averaging between all values, we obtain  $\Delta E_{e,bind} = -41.8 \pm 8.6$  kJ mol<sup>-1</sup>, to which we attach a conservative uncertainty taken as twice the standard deviation. We can convert the above electronic binding energy to a binding energy at 0 K using the zero-point vibrational energies (ZPVEs) calculated within the rigid rotor-harmonic oscillator approximation at the PBE0-D3BJ/6-31G

(d) level of theory. Scaling the harmonic ZPVEs by 0.9733 as recommended in Ref. [60] results in a binding energy at 0 K of  $\Delta H_{0,bind} = -41.0 \pm 8.6$  kJ mol<sup>-1</sup>. An experimental bonding energy between benzene and the basal plane of highly oriented pyrolytic graphite has been obtained from thermal desorption spectroscopy. These experiments result in binding energies of  $-48.2 \pm 7.7$  and  $-46.4$  kJ mol<sup>-1</sup>. [21,22] An uncertainty has not been reported for the later value, however, this experimental determination was obtained over 50 years ago and is likely to carry an uncertainty larger than the one assigned to the more recent experimental value. Thus, our best theoretical value of  $\Delta H_{0,bind} = -41.0 \pm 8.6$  kJ mol<sup>-1</sup> agrees with the experimental values to within overlapping uncertainties.

#### 4. Conclusions

We address the issues associated with predicting an accurate binding energy between graphene and benzene from DFT-D4 calculations using a series of increasingly larger nanographenes (C<sub>24</sub>H<sub>12</sub>, C<sub>54</sub>H<sub>18</sub>, C<sub>96</sub>H<sub>24</sub>, C<sub>150</sub>H<sub>30</sub>, and C<sub>216</sub>H<sub>36</sub>). We consider four dispersion-corrected DFT methods from the upper rungs of Jacob's Ladder that were developed for accurate prediction of noncovalent interactions. Specifically, the global hybrid PBE0-D4, range-separated hybrid  $\omega$ B97X-D4, and hybrid-meta GGA/NGA methods PW6B95-D4 and MN15. These methods include varying degrees of global and range-separated exact Hartree-Fock exchange. With regard to the convergence of the binding energy with respect to the size of the nanographene, we draw the following conclusions:

- The C<sub>24</sub>H<sub>12</sub> nanographene underestimates the binding energies obtained for the largest C<sub>216</sub>H<sub>36</sub> nanographene by large amounts of up to 13.0 kJ mol<sup>-1</sup> and should not be used as a model for nanographene.
- The C<sub>54</sub>H<sub>18</sub> nanographene still underestimates the best binding energies by chemically significant amounts of up to 3.7 kJ mol<sup>-1</sup>.
- The C<sub>96</sub>H<sub>24</sub> model is the smallest nanographene that gives chemically accurate binding energies with benzene relative to the largest C<sub>216</sub>H<sub>36</sub> nanographene. For all DFT methods, the deviations between the two nanographene model systems are below 1.4 kJ mol<sup>-1</sup>.
- The C<sub>150</sub>H<sub>30</sub> nanographene results in binding energies that are practically indistinguishable from those obtained for the C<sub>216</sub>H<sub>36</sub> nanographene, with deviations smaller than 0.3 kJ mol<sup>-1</sup> for all DFT methods.
- The rate of convergence with respect to the size of the nanographene varies between the considered DFT methods, with MN15 and PBE0-D4 representing limit cases of faster and slower convergence rates, respectively.

In terms of the best theoretical binding energy, we offer the following conclusions:

- The electronic binding energies for the most extensive benzene $\bullet\bullet\bullet$ C<sub>216</sub>H<sub>36</sub> model system are  $\Delta E_{e,bind} = -37.9$  (MN15),  $-39.7$  ( $\omega$ B97X-D4),  $-40.7$  (PW6B95-D4), and  $-49.1$  (PBE0-D4) kJ mol<sup>-1</sup>.
- Averaging between the above values, we obtain  $\Delta E_{e,bind} = -41.8 \pm 8.6$  kJ mol<sup>-1</sup>, to which we attach a conservative uncertainty taken as twice the standard deviation.
- The theoretical binding energy at 0 K ( $\Delta H_{0,bind} = -41.0 \pm 8.6$  kJ mol<sup>-1</sup>) agrees with the experimental value of  $-48.2 \pm 7.7$  kJ mol<sup>-1</sup> within overlapping uncertainties.

#### CRedit authorship contribution statement

**Amir Karton:** Conceptualization, Methodology, Software, Data curation, Investigation, Writing – review & editing.

## Declaration of Competing Interest

The authors declare that they have no known competing financial interests or personal relationships that could have appeared to influence the work reported in this paper.

## Acknowledgement

We gratefully acknowledge the generous allocation of computing time from the National Computational Infrastructure (NCI) National Facility and system administration support provided by the Faculty of Science at UWA to the Linux cluster of the Karton group. A.K. gratefully acknowledges an Australian Research Council (ARC) Future Fellowship (Project No. FT170100373).

## Data availability statement

The data supporting this study's findings are available within the article and its supplementary material and from the corresponding author upon reasonable request.

## Appendix A. Supplementary material

Def2-TZVP-full-CP electronic binding energies for PBE0-D4,  $\omega$ B97X-D4, PW6B95-D4, and MN15 (Table S1); the difference between the Def2-TZVP-half-CP and Def2-TZVP-full-CP electronic binding energies for PBE0-D4,  $\omega$ B97X-D4, PW6B95-D4, and MN15 (Table S2); PBE0-D3(BJ)/6-31G(d) optimized structures for all the monomers and dimers considered in the present work (Table S3); harmonic frequencies for all the monomers and dimers considered in the present work (Table S4). Supplementary data to this article can be found online at <https://doi.org/10.1016/j.chemphys.2022.111606>.

## References

- [1] L.H. Fan, H.Y. Ge, S.Q. Zou, Y. Xiao, H.G. Wen, Y. Li, H. Feng, M. Nie, Sodium alginate conjugated graphene oxide as a new carrier for drug delivery system, *Int. J. Biol. Macromol.* 93 (2016) 582.
- [2] H.Y. Mao, S. Laurent, W. Chen, O. Akhavan, M. Imani, A.A. Ashkarran, M. Mahmoudi, Graphene: promises, facts, opportunities, and challenges in nanomedicine, *Chem. Rev.* 113 (2013) 3407.
- [3] S.S.N. Azman, N.W.M. Zulkifli, H.H. Masjuki, M. Gulzar, R. Zahid, Study of tribological properties of lubricating oil blend added with graphene nanoplatelets, *J. Mater. Res.* 24 (2016) 1932.
- [4] S. Gowtham, R.H. Scheicher, R. Ahuja, R. Pandey, S.P. Karna, *Phys. Rev. B* 76 (2007) 033401.
- [5] A. Piras, C. Ehlert, G. Gryn'ova, Sensing and sensitivity: computational chemistry of graphene-based sensors, *Wiley Interdiscip. Rev.: Comput. Mol. Sci.* (2021) e1526.
- [6] S. Hou, X. Wu, Y. Lv, W. Jia, J. Guo, L. Wang, F. Tong, D. Jia, Ultralight, highly elastic and bioinspired capillary-driven graphene aerogels for highly efficient organic pollutants absorption, *Appl. Surf. Sci.* 509 (2020) 144818.
- [7] C.H. Guan, X.J. Lv, Z.X. Han, C. Chen, Z.M. Xu, Q.S. Liu, The adsorption enhancement of graphene for fluorine and chlorine from water, *Appl. Surf. Sci.* 516 (2020) 146157.
- [8] V. Georgakilas, M. Otyepka, A.B. Bourlinos, V. Chandra, N. Kim, K.C. Kemp, P. Hobza, R. Zboril, K.S. Kim, *Chem. Rev.* 112 (2012) 6156.
- [9] A. Rochefort, J.D. Wuest, Interaction of substituted aromatic compounds with graphene, *Langmuir* 25 (2009) 210.
- [10] G. García, M. Atilhan, S. Aparicio, Flavonols on graphene: a DFT insight, *Theor. Chem. Acc.* 134 (2015) 57.
- [11] S.D. Chakarova-Käck, E. Schröder, B.I. Lundqvist, D.C. Langreth, Application of van der Waals density functional to an extended system: adsorption of benzene and naphthalene on graphite, *Phys. Rev. Lett.* 96 (2006) 146107.
- [12] J. Björk, F. Hanke, C.A. Palma, P. Samori, M. Cecchini, M. Persson, Adsorption of aromatic and anti-aromatic systems on graphene through  $\pi$ - $\pi$  stacking, *J. Phys. Chem. Lett.* 1 (2010) 3407.
- [13] O.V. Ershova, T.C. Lillestolen, E. Bichoutskaia, Study of polycyclic aromatic hydrocarbons adsorbed on graphene using density functional theory with empirical dispersion correction, *Phys. Chem. Chem. Phys.* 12 (2010) 6483.
- [14] S. Wangmo, R. Song, L. Wang, W. Jin, D. Ding, Z. Wang, R.Q. Zhang, Strong interactions and charge transfers between a charged phenyl molecule and multilayer graphenes, *J. Mater. Chem.* 22 (2012) 23380.
- [15] S.M. Kozlov, F. Viñes, A. Görling, On the interaction of polycyclic aromatic compounds with graphene, *Carbon* 50 (2012) 2482.
- [16] K. Berland, P. Hylgaard, Analysis of van der Waals density functional components: binding and corrugation of benzene and C<sub>60</sub> on boron nitride and graphene, *Phys. Rev. B: Condens. Matter Mater. Phys.* 87 (2013) 205421.
- [17] C. Lechner, A.F. Sax, Adhesive forces between aromatic molecules and graphene, *J. Phys. Chem. C* 118 (2014) 20970.
- [18] C. Lechner, A.F. Sax, Towards atomic-level mechanics: adhesive forces between aromatic molecules and carbon nanotubes, *Appl. Surf. Sci.* 420 (2017) 606.
- [19] X. Zhang, J. Guo, W. Zhao, Experimental measurement and theoretical prediction of the adhesion force between a single phenyl ring and graphene, *Appl. Surf. Sci.* 545 (2021) 148980.
- [20] X. Zhang, J. Guo, Adsorption, stability and evolution path of benzene on graphene surface: size and edge effects, *Appl. Surf. Sci.* 571 (2022) 151376.
- [21] R. Zacharia, H. Ulbricht, T. Hertel, Interlayer cohesive energy of graphite from thermal desorption of polyaromatic hydrocarbons, *Phys. Rev. B* 69 (2004) 155406.
- [22] C. Pierce, Localized adsorption on graphite and absolute surface areas, *J. Phys. Chem.* 78 (1969) 813.
- [23] D.C. Langreth, M. Dion, H. Rydberg, E. Schroder, P. Hylgaard, B.I. Lundqvist, van der Waals density functional with applications, *Int. J. Quantum Chem.* 101 (2005) 599.
- [24] A. Tkatchenko, M. Scheffler, Accurate molecular van der Waals interactions from ground-state electron density and free-atom reference data, *Phys. Rev. Lett.* 102 (2009) 073005.
- [25] J.P. Perdew, K. Burke, M. Ernzerhof, Generalized gradient approximation made simple, *Phys. Rev. Lett.* 77 (1996) 3865.
- [26] C. Adamo, V. Barone, Toward reliable density functional methods without adjustable parameters: the PBE0 model, *J. Chem. Phys.* 110 (13) (1999) 6158-6170.
- [27] J.-D. Chai, M. Head-Gordon, Systematic optimization of long-range corrected hybrid density functionals, *J. Chem. Phys.* 128 (2008) 084106.
- [28] Y. Zhao, D.G. Truhlar, Design of density functionals that are broadly accurate for thermochemistry, thermochemical kinetics, and nonbonded interactions, *J. Phys. Chem. A* 109 (2005) 5656.
- [29] H.S. Yu, X. He, S.L. Lia, D.G. Truhlar, MN15: A Kohn-Sham global-hybrid exchange-correlation density functional with broad accuracy for multi-reference and single-reference systems and noncovalent interactions, *Chem. Sci.* 7 (2016) 5032.
- [30] E. Caldeweyher, S. Ehlert, A. Hansen, H. Neugebauer, S. Spicher, C. Bannwarth, S. Grimme, A generally applicable atomic-charge dependent London dispersion correction, *J. Chem. Phys.* 150 (2019) 154122.
- [31] E. Caldeweyher, C. Bannwarth, S. Grimme, Extension of the D3 dispersion coefficient model, *J. Chem. Phys.* 147 (2017) 034112.
- [32] A. Karton, D. Gruzman, J.M.L. Martin, Benchmark thermochemistry of the C<sub>n</sub>H<sub>2n+2</sub> alkane isomers (n = 2-8) and performance of DFT and composite ab initio methods for dispersion-driven isomeric equilibria, *J. Phys. Chem. A* 113 (2009) 8434.
- [33] S. Grimme, J. Antony, S. Ehrlich, H. Krieg, A consistent and accurate ab initio parametrization of density functional dispersion correction (DFT-D) for the 94 elements H-Pu, *J. Chem. Phys.* 132 (2010) 154104.
- [34] L. Goerigk, S. Grimme, A thorough benchmark of density functional methods for general main group thermochemistry, kinetics, and noncovalent interactions, *Phys. Chem. Chem. Phys.* 13 (2011) 6670.
- [35] S. Grimme, S. Ehrlich, L. Goerigk, Effect of the damping function in dispersion corrected density functional theory, *J. Comput. Chem.* 32 (2011) 1456.
- [36] L. Goerigk, A. Hansen, C. Bauer, S. Ehrlich, A. Najibi, S. Grimme, A look at the density functional theory zoo with the advanced GMTKN55 database for general main group thermochemistry, kinetics and noncovalent interactions, *Phys. Chem. Chem. Phys.* 19 (2017) 32184.
- [37] A. Karton, How reliable is DFT in predicting relative energies of polycyclic aromatic hydrocarbon isomers? Comparison of functionals from different rungs of Jacob's ladder, *J. Comput. Chem.* 38 (2017) 370.
- [38] M. Ha, D.Y. Kim, N. Li, J.M.L. Madridejos, I.K. Park, I.S. Youn, J. Lee, C. Baig, M. Filatov, S.K. Min, G. Lee, K.S. Kim, Adsorption of carbon tetrahalides on coronene and graphene, *J. Phys. Chem. C* 121 (2017) 14968.
- [39] J. Antony, R. Sure, S. Grimme, Using dispersion-corrected density functional theory to understand supramolecular binding thermodynamics, *Chem. Commun.* 51 (2015) 1764.
- [40] S. Grimme, Density functional theory with London dispersion corrections, *Wiley Interdiscip. Rev.: Comput. Mol. Sci.* 1 (2) (2011) 211-228.
- [41] A.D. Becke, E.R. Johnson, A density-functional model of the dispersion interaction, *J. Chem. Phys.* 123 (2005) 154101.
- [42] F. Weigend, R. Ahlrichs, Balanced basis sets of split valence, triple zeta valence and quadruple zeta valence quality for H to Rn: design and assessment of accuracy, *Phys. Chem. Chem. Phys.* 7 (18) (2005) 3297.
- [43] S.F. Boys, F. Bernardi, Calculation of small molecular interactions by differences of separate total energies - some procedures with reduced errors, *Mol. Phys.* 19 (1970) 553.
- [44] L.A. Burns, M.S. Marshall, C.D. Sherrill, Comparing counterpoise-corrected, uncorrected, and averaged binding energies for benchmarking noncovalent interactions, *J. Chem. Theory Comput.* 10 (2014) 49.
- [45] B. Brauer, M.K. Kesharwani, J.M.L. Martin, Some observations on counterpoise corrections for explicitly correlated calculations on noncovalent interactions, *J. Chem. Theory Comput.* 10 (2014) 3791.
- [46] M. J. Frisch, G. W. Trucks, H. B. Schlegel, G. E. Scuseria, M. A. Robb, J. R. Cheeseman, G. Scalmani, V. Barone, G. A. Petersson, H. Nakatsuji, X. Li, M. Caricato, A. V. Marenich, J. Bloino, B. G. Janesko, R. Gomperts, B. Mennucci, H. P. Hratchian, J. V. Ortiz, A. F. Izmaylov, J. L. Sonnenberg, D. Williams-Young, F. Ding, F. Lipparini, F. Egidi, J. Goings, B. Peng, A. Petrone, T. Henderson, D. Ranasinghe, V. G. Zakrzewski, J. Gao, N. Rega, G. Zheng, W. Liang, M. Hada, M. Ehara, K. Toyota, R. Fukuda, J. Hasegawa, M. Ishida, T. Nakajima, Y. Honda, O. Kitao, H. Nakai, T. Vreven, K. Throssell, J. A. Montgomery, Jr., J. E. Peralta, F.

- Ogliaro, M. J. Bearpark, J. J. Heyd, E. N. Brothers, K. N. Kudin, V. N. Staroverov, T. A. Keith, R. Kobayashi, J. Normand, K. Raghavachari, A. P. Rendell, J. C. Burant, S. S. Iyengar, J. Tomasi, M. Cossi, J. M. Millam, M. Klene, C. Adamo, R. Cammi, J. W. Ochterski, R. L. Martin, K. Morokuma, O. Farkas, J. B. Foresman, D.J. Fox, Gaussian 16, Revision A.03, Gaussian, Inc., Wallingford, CT, 2016.
- [47] A.A. Kroeger, A. Karton, Graphene-induced planarization of cyclooctatetraene derivatives, *J. Comput. Chem.* 43 (2022) 96.
- [48] A. A. Kroeger, A. Karton,  $\pi$ - $\pi$  catalysis in carbon flatland—flipping [8]annulene on graphene, *Chem. Eur. J.* 27 (2021) 3420.
- [49] O. Yönder, G. Schmitz, C. Hättig, R. Schmid, P. Debiagi, C. Hasse, A. Locaspi, T. Faravelli, Can small polyaromatics describe their larger counterparts for local reactions? A computational study on the H-abstraction reaction by an H-atom from polyaromatics, *J. Phys. Chem. A* 124 (2020) 9626.
- [50] A. Karton, Catalysis on pristine 2D materials via dispersion and electrostatic interactions, *J. Phys. Chem. A* 124 (2020) 6977.
- [51] A.A. Kroeger, A. Karton, Catalysis by pure graphene—from supporting actor to protagonist through shape complementarity, *J. Org. Chem.* 84 (2019) 11343.
- [52] E. Zarudnev, S. Stepanian, L. Adamowicz, V. Karachevtsev, Noncovalent interaction of graphene with heterocyclic compounds: Benzene Imidazole, Tetracene, and Imidazophenazines, *ChemPhysChem* 17 (2016) 1204.
- [53] P.A. Denis, Pristine graphene-based catalysis: significant reduction of the inversion barriers of adsorbed and confined corannulene, sumanene, and dibenzo[a, g] corannulene, *J. Phys. Chem. A* 119 (2015) 5770.
- [54] A. Karton, Inversion and rotation processes involving nonplanar aromatic compounds catalyzed by extended polycyclic aromatic hydrocarbons, *Chem. Phys. Lett.* 614 (2014) 156.
- [55] C. Feng, C. S. Lin, W. Fan, R. Q. Zhang, M. A. Van Hove, Stacking of polycyclic aromatic hydrocarbons as prototype for graphene multilayers, studied using density functional theory augmented with a dispersion term, *J. Chem. Phys.* 131 (2009) 194702.
- [56] I.D. Mackie, G.A. DiLabio, Interactions in large, polyaromatic hydrocarbon dimers: application of density functional theory with dispersion corrections, *J. Phys. Chem. A* 112 (2008) 10968.
- [57] P.B. Karadakov, Do large polycyclic aromatic hydrocarbons and graphene bend? How popular theoretical methods complicate finding the answer to this question, *Chem. Phys. Lett.* 646 (2016) 190.
- [58] A. Karton, J.M.L. Martin, Prototypical  $\pi$ - $\pi$  dimers re-examined by means of high-level CCSDT(Q) composite ab initio methods, *J. Chem. Phys.* 154 (2021) 124117.
- [59] A. Karton, A computational chemist's guide to accurate thermochemistry for organic molecules, *Wiley Interdiscip. Rev.: Comput. Mol. Sci.* 6 (3) (2016) 292–310.
- [60] M.K. Kesharwani, B. Brauer, J.M.L. Martin, Frequency and zero-point vibrational energy scale factors for double-hybrid density functionals (and other selected methods): can anharmonic force fields be avoided? *J. Phys. Chem. A* 119 (2015) 1701.